

# Investigation of mass transfer, thermodynamics, and greenhouse gases properties in pennyroyal drying

Mohammad Kaveh<sup>1</sup>  | Hamed Karami<sup>1,2</sup>  | Ahmad Jahanbakhshi<sup>1</sup> 

<sup>1</sup>Department of Biosystems Engineering, University of Mohaghegh Ardabili, Ardabil, Iran

<sup>2</sup>Department of Farm Technology, Wageningen University & Research, Wageningen, Netherlands

## Correspondence

Mohammad Kaveh and Hamed Karami, Department of Biosystems Engineering, University of Mohaghegh Ardabili, Ardabil, Iran.

Email: hamed.karami@wur.nl; hamedkarami@uma.ac.ir (H. K.) and sirwankaweh@gmail.com; sirwankaweh@uma.ac.ir (M. K)

## Abstract

In this research, kinetic analysis, energy, exergy, and greenhouse gases of a hybrid laboratory dryer (solar-hot air) are presented for pennyroyal. Drying was performed at input temperatures of 50, 60, and 70°C and air velocities of 0.6, 1.2, and 1.8 m/s. The effect of drying variables on moisture ratio, effective moisture diffusivity, specific energy consumption, energy utilization ratio, energy utilization, exergy efficiency, and exergy loss was investigated. The highest amounts of effective moisture diffusivity and specific energy consumption were  $2.30 \times 10^{-10} \text{ m}^2/\text{s}$  and 48.60 kWh/kg, respectively. Energy utilization and energy utilization ratio varied from 0.0064 to 0.0826 kJ/s and from 0.056 to 0.957, respectively. Exergy loss and exergy efficiency varied between 0.0037 to 0.0510 kJ/s and 0.2428 to 0.8731, respectively. In addition, by increasing the temperature and intake air velocity, drying rate increased and the emissions of greenhouse gases ( $\text{CO}_2$ ,  $\text{SO}_2$ , and  $\text{NO}_x$ ) were reduced.

## Practical Applications

Modeling of the drying process is an important aspect of drying technology, especially in drying for industrial purposes. The aim of modeling is to select the most suitable drying method and the best operating conditions for obtaining the product. Some of the key issues in drying have been to reduce the price of the energy resources used, increase the drying efficiency, and improve the quality of the dried products. The concept of exergy is defined by the concept of reversible work. The concept of reversibility depends on energy balance and mass regardless of energy quality (exergy loss).

## 1 | INTRODUCTION

Pennyroyal belongs to the family of *Lamiaceae* plants and is of great importance in cosmetic, food, and medical industries. *Nepeta L.* genus of the pennyroyals is one of the major genera in the *Lamiaceae* family (Hassanpouraghdam & Hassani, 2014). To date, 250 species of this genus have been reported in the world and 67 species have been reported in Iran.

Drying is one of the oldest methods for preserving agricultural products. Thus, it is of utmost importance in processing herbs

because if essential herbs are not dried immediately or their essence is not extracted on time, they will lose their effective ingredients and their volatile compounds (Abbaspour-Gilandeh, Kaveh, & Jahanbakhshi, 2019; Sun, Zhang, & Mujumdar, 2019). Drying the plant immediately after harvest would help preservation of its color and aroma.

Exergy and energy analysis is applied to determine the amount of energy needed to dry the product and exergy loss at each stage of the process. Therefore, exergy and energy analysis is important (Fudholi, Sopian, Othman, & Ruslan, 2014). The concept of exergy

This is an open access article under the terms of the Creative Commons Attribution License, which permits use, distribution and reproduction in any medium, provided the original work is properly cited.

© 2020 The Authors. *Journal of Food Process Engineering* published by Wiley Periodicals LLC.

is defined using the concept of reversible work. The concept of reciprocity, regardless of the reduction of energy quality (energy dissipation), depends on the balance of energy and mass (Abbaspour-Gilandeh, Jahanbakhshi, & Kaveh, 2020; Akpinar, Midilli, & Bicer, 2006).

Recently, several studies have been carried out to analyze energy and exergy emissions in the process of drying products such as red seaweed in a solar dryer (Fudholi et al., 2014), soybeans in microwave-assisted fluidized bed dryer (Ranjbaran & Zare, 2013), carrot in heat pump and infrared–heat pump dryer (Aktas, Khanlari, Amini, & Sevik, 2017), turmeric slices in microwave (Surendhar, Ivasubramanian, Vidhyeswari, & Deepanraj, 2018), quince slice in a convective dryer (Abbaspour-Gilandeh et al., 2020), orange slices in microwave with osmotic pretreatment (Azadbakht, Torshizi, Noshad, & Rokhbin, 2018), banana slices in forced convective dryer (Taheri-Garavand, Karimi, Karimi, Lotfi, & Khoobbakht, 2018), Kodo millet grains and Fenugreek seeds in a fluidized bed dryer (Yogendrasasidhar & Setty, 2018), and mushroom in a fluidized-bed dryer with osmotic pretreatment (Darvishi, Azadbakht, & Noralahi, 2018).

Greenhouse gases are gases that act as a barrier to prevent heat from leaving the atmosphere and thus cause global warming. Over the past 100 years, the accumulation of greenhouse gases in the atmosphere has increased the temperature of the Earth's surface and continues to have unknown effects on the Earth's climate in the future (Khoshnevisan, Rafiee, Omid, & Mousazadeh, 2013). Six important greenhouse gases are carbon dioxide, methane, nitrous oxide, hydrofluorocarbons (HFCs), perhydro-fluorocarbons, and sulfur hexafluoride (Ahmadi, Rozkshosh, & Haghhighifard, 2014). The burning of fossil fuels such as diesel and gasoline, the change in land use from forests and pastures to agricultural and residential land as well as a number of post-harvest processes for crops are the main causes of increased greenhouse gas emissions (Samani, Choobin, Ghasemi-Varnamkhasti, & Abedi, 2018).

Nazari et al. (2010) reported that the total  $\text{SO}_2$ ,  $\text{CO}_2$ , and  $\text{NO}_x$  emissions of Iranian power plants using different fuels were 125.34, 0.255, and 0.465 Tg.

Motevali and Tabatabaei (2017) studied energy consumption and GHG emissions ( $\text{CO}_2$ ,  $\text{SO}_2$ , and  $\text{NO}_x$ ) for the drying of rose flowers in different dryers (hot air, infrared, infrared-hot air, microwave, microwave-hot air, vacuum and solar). According to their findings, by increasing air temperature at inlet, infrared power and microwave power, specific energy consumption, and greenhouse gas emissions were reduced. Also, these two parameters were increased by increasing the air velocity.

However, the data reported on energy, exergy, and greenhouse gas emission analyses in the process of drying herbal plants are very few. Given the importance of the pennyroyal plant and its sensitivity to heat application in the drying process, the aims of this research are to optimize the plant's drying conditions, modeling, evaluation and analysis of kinetics, effective moisture diffusion coefficient, activation energy, energy, exergy, and emission of greenhouse gases using a hybrid dryer (solar- hot air).

## 2 | MATERIALS AND METHODS

### 2.1 | Experiments

In this research, leaves and twigs of pennyroyal plant (*Mentha pulegium L.*) were harvested. The experiments were carried out at four temperatures of 40, 50, 60, and 70°C and three levels of input air velocity: 0.6, 1.2, and 1.8 m/s with three replications.

The dryer used in this study included a solar collector with a 1,000 watt electric element for heating the input air to the drying chamber and five temperature sensors (LM75) with a range of measurements from  $-55$  to  $125^\circ\text{C}$  and the measurement accuracy of  $\pm 2^\circ\text{C}$  (Figure 1) (Karami, Kaveh, Mirzaee-Ghaleh, & Taghinezhad, 2018). The position of the sensors was arranged as three sensors on the collector, a sensor at the air inlet into the chamber, a sensor inside the chamber, and a sensor at the air outlet from the chamber. Two humidity sensors (HS1101) with the precision of  $\pm 2\%$  were also used to measure the relative humidity of air displacement. Humidity sensors were located at the inlet and outlet inside the chamber. The dryer's fan had the ability to change the amount of the input air that entered the drying chamber. To measure the speed of the airflow to the dryer chamber, a speedometer of the model AVM-07 made in Taiwan was used with a measurement accuracy of 0.1 m/s. To implement the drying process, the ATMEGA 8 model of AVR microcontroller made in China was used (Karami, Rasekh, Darvishi, & Khaledi, 2017).

In order to do the experiments, 200 g of pennyroyal leaves and twigs were placed in a single layer on the dryer's mesh tray. During the drying process, the product weight changes were recorded by a digital scale (GF-3000, AND) with a precision of  $\pm 0.01$  g. This scale was attached directly to the trays so that the samples did not need to be brought out of the chamber for weighing. The final moisture content of the samples was then calculated using the oven dryer at 70°C for 24 hours through the following equation (Zhao et al., 2018):

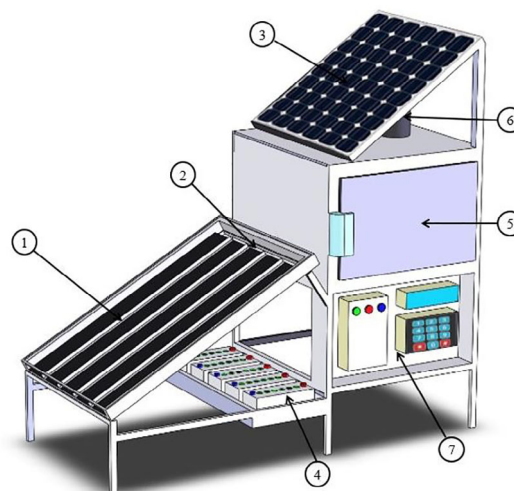


**FIGURE 1** Structure of the dryer: (1) solar collector; (2) electric element; (3) solar cell; (4) batteries; (5) drying chamber; (6) damper; and (7) controller box

$$MC_{db} = \frac{W_i - W_d}{W_d} \quad (1)$$

To achieve system stability, all tests started 25 min after the system was turned on. Then, the tray containing the samples was placed in the drying chamber. The process of drying went on like this: the fan transferred the air heated by an electric heater from the collector to the trays. The flow of air absorbed the sample's moisture as it passed through it and dried the plant. In addition, increase in temperature led to the rapid escape of moisture from the sample's texture and thus dried the product.

As laboratory data used for the process of drying pennyroyal plant two parameters of moisture ratio (MR) and drying rate were taken into account which were calculated through the following equations (Abbaspour-Gilandeh et al., 2020:

$$MR = \frac{M_t - M_e}{M_o - M_e} \quad (2)$$

$$DR = \frac{MC_{t+dt} - MC_t}{dt} \quad (3)$$

Due to the low value of  $M_e$  compared to  $M_t$  and  $M_o$ , Equation (2) can be simplified as  $MR = \frac{M_t}{M_o}$  (Badaoui, Hanini, Djebli, Brahim, & Benhamou, 2019). In order to model pennyroyal's moisture in the process of drying in the hybrid dryer (solar-hot air), known models that are frequently applied in the processes of drying agricultural products were used in this study (Table 1). The three criteria of determination coefficient ( $R^2$ ), root mean square error (RMSE), and chi-square ( $\chi^2$ ) were used to evaluate the best model according to the following equations:

$$R^2 = 1 - \frac{\sum_{i=1}^N [MR_{exp,i} - MR_{pre,i}]^2}{\sum_{k=1}^N \left[ \frac{\sum_{k=1}^n MR_{pre,i}}{N} - MR_{pre,i} \right]^2} \quad (4)$$

$$\chi^2 = \frac{\sum_{i=1}^N (MR_{exp,i} - MR_{pre,i})^2}{N - z} \quad (5)$$

$$RMSE = \left[ \frac{1}{N} \sum_{i=1}^N (MR_{pre,i} - MR_{exp,i})^2 \right]^{\frac{1}{2}} \quad (6)$$

## 2.2 | Effective moisture diffusion coefficient ( $D_{eff}$ )

Fick's second law (Equation (7)) is widely used to describe diffusion in the process of drying agricultural products (Mohammadi, Tabatabaekolour, & Motevali, 2019):

$$\frac{\partial M}{\partial t} = D_{eff} \frac{\partial^2 M}{\partial x^2} \quad (7)$$

After expanding Equation (7) and applying the drying conditions for a long time, Equation (8) was obtained to determine the diffusion coefficient (Zhao et al., 2018):

$$MR = \frac{M_t - M_e}{M_o - M_e} = \frac{8}{\pi^2} \sum_{n=0}^{\infty} \frac{1}{(2n+1)^2} \exp\left(- (2n-1)^2 \pi^2 \frac{D_{eff} t}{L^2}\right) \quad (8)$$

The effective moisture diffusion coefficient was obtained using Equation (9) from the gradient (K) of the Ln (MR) graph over time:

**TABLE 1** Mathematical models to fit the experimental data

Models	Equations	References
Newton (Lewis)	$MR = \exp(-kt)$	Ghnimi, Hassini, and Bagane (2016)
Page	$MR = \exp(-kt^n)$	Atalay, Çoban, and Kincay (2017)
Logarithmic	$MR = a \exp(-kt) + c$	Zhao et al. (2018)
Henderson and Pabis	$MR = a \exp(-kt)$	Abbaspour-Gilandeh et al. (2019)
Modified Henderson and Pabis	$MR = a \exp(-kt) + b \exp(-gt) + c \exp(-ht)$	Sehrawat, Nema, and Kaur (2018)
Two-term	$MR = a \exp(-k_0t) + b \exp(-k_1t)$	Ghnimi et al. (2016)
Two-term exponential	$MR = a \exp(-kt) + (1 - a)\exp(-kat)$	Kaveh, Jahanbakhshi, Abbaspour-Gilandeh, Taghinezhad, and Moghimi (2018)
Midilli et al.	$MR = a \exp(-kt^n) + bt$	Abbaspour-Gilandeh et al. (2020)
Verma et al.	$MR = a \exp(-kt) + (1 - a) \exp(-gt)$	Badaoui et al. (2019)
Wang and Singh	$MR = 1 + at + bt^2$	Atalay et al. (2017)
Approximation of diffusion	$MR = a \exp(-kt) + (1 - a) \exp(-kbt)$	Wang, Li, Hassani, Wang, and Yang (2018)
Demir et al.	$MR = a \exp(-kt)^n + b$	Kaveh et al. (2020)
Logistic	$MR = a/(1 + b \exp(kt))$	Jahanbakhshi, Kaveh, Taghinezhad, and Sharabiani (2020)
Parabolic	$MR = a + bt + ct^2$	Abbaspour-Gilandeh et al. (2019)

$$K = \frac{\pi^2 D_{eff}}{4L^2} \quad (9)$$

$$\dot{Q}_{evap} = \dot{m}_{ai} h_{fg} w \quad (18)$$

## 2.3 | Activation energy

Activation energy for different temperatures and velocities was calculated using the following equation (Atalay et al., 2017):

$$D_{eff} = D_0 \exp\left(-\frac{E_a}{R_g T_{abs}}\right) \quad (10)$$

To obtain  $E_a$  linear relationship, Equation (11) was used.

$$\ln(D_{eff}) = \ln(D_0) - \left(\frac{E_a}{R_g}\right) \left(\frac{1}{T_{abs}}\right) \quad (11)$$

By charting  $\ln(D_{eff})$  against  $\frac{1}{T_{abs}}$ , a line with slope  $K_2$  was obtained.

$$K_2 = \left(\frac{E_a}{R_g}\right) \quad (12)$$

## 2.4 | Energy analysis

In this study, energy utilization (EU) during the process of drying pen-nyroyal was calculated using the following equation (Aghbashlo, Kianmehr, & Arabhosseini, 2008):

$$EU = \dot{m}_{ai} h_{ai} + \dot{m}_{PF} h_{PF} - \dot{m}_{ao} h_{ao} - \dot{m}_{PD} h_{PD} - \dot{Q}_{defl} \quad (13)$$

Relations (14)–(16) were used to obtain the input and output air flows and air density, respectively (Taheri-Garavand et al., 2018):

$$\dot{m}_{ai} = \dot{m}_{ao} \quad (14)$$

$$\dot{m}_a = \rho_a U_a A_{dc} \quad (15)$$

$$\rho_a = \frac{P}{RT} \quad (16)$$

The enthalpy of the input or output air is equal to the dry air enthalpy plus the enthalpy of the water vapor. Having obtained these indices exergy loss was calculated through the following equation (Corzo, Bracho, Vasquez, & Pereira, 2008):

$$h_a = C_a (T_a - T_{\infty}) + h_{fg} w \quad (17)$$

The heat transfer rate, which leads to evaporation in the dryer, was obtained through the following equation (Nazghelichi, Kianmehr, & Aghbashlo, 2010):

In order to obtain the enthalpy of the fresh and dried product, the specific heat of the input or output product had to be first calculated from Equation (19) and the temperature of the input or output product as well as the ambient temperature was measured using a thermometer (Aghbashlo et al., 2008):

$$h_p = C_p (T_p - T_{\infty}) \quad (19)$$

However, in the wet state, the amount of the input and output air moisture should also be available. This factor is used to determine the input or output air enthalpy (Equation (20)) (Motevali & Minaee, 2012):

$$C_a = 1.004 + 1.88w \quad (20)$$

The rate of heat dissipated from the output air depends on the flow rates of the input air, the specific heat of the input air, and the temperature of the input and output air. The rate of heat dissipated from the output air can be obtained using the following equation (Akpinar, 2010):

$$\dot{Q}_{aol} = \dot{m}_{ai} C_{ai} (T_{ai} - T_{ao}) \quad (21)$$

The heat loss rate from the dryer's body can be obtained from the following equation (Nazghelichi et al., 2010):

$$\dot{Q}_{defl} = U_{def} A_{def} (T_{mvdef} - T_{\infty}) \quad (22)$$

Finally, the heat loss coefficient of the dryer body can be obtained by equating Equations (21) and (22). As mentioned before, the heat loss coefficient of the dryer body can be obtained by using the following equation (Aghbashlo et al., 2008; Akpinar, 2010):

$$U_{def} = \frac{\dot{m}_{ai} c_{ai} (T_{ai} - T_{ao})}{A_{def} (T_{mvdef} - T_{\infty})} \quad (23)$$

Eventually, the energy utilization ratio (EUR) was determined by (Aghbashlo et al., 2008):

$$EUR = \frac{\dot{m}_{ai} h_{ai} + \dot{m}_{PF} h_{PF} - \dot{m}_{ao} h_{ao} - \dot{m}_{PD} h_{PD} - \dot{Q}_{defl}}{\dot{m}_{ai} (h_{ai} - h_{\infty})} \quad (24)$$

## 2.5 | Exergy analysis

The total exergy of the input and output air for the fresh and dry product can be calculated by the second law of thermodynamics. The basic method for analyzing the exergy of the drying chamber is to

calculate the exergy in stable conditions. For this goal, the general form of the exergy equation for stable conditions can be used. The exergy of the input or output air and the exergy of the input or output product can be obtained through the following equation (Ergün, Ceylan, Acar, & Erkamaz, 2017):

$$Ex = \dot{m}C \left[ (T - T_{\infty}) - T_{\infty} \ln \left( \frac{T}{T_{\infty}} \right) \right] \quad (25)$$

The most important step in the exergy analysis is measuring the amount of exergy rate from the dryer's body, which was calculated using the following equation (Rabha, Muthukumar, & Somayaji, 2017):

$$EX_{defl} = \left( 1 - \left( \frac{T_{\infty}}{T_{mvdef}} \right) \right) \dot{Q}_{defl} \quad (26)$$

Relations (27)–(29) were used to obtain the amount of exergy loss from the dryer's body (Aktas et al., 2017; Darvishi et al., 2018):

$$\sum EX_i = \sum EX_i - \sum EX_o \quad (27)$$

$$\sum EX_i = EX_{ai} + EX_{PF} \quad (28)$$

$$EX_o = EX_{ao} + EX_{PD} + EX_{defl} \quad (29)$$

Finally, the exergy efficiency was calculated according to the following equation (Abbaspour-Gilandeh et al., 2020; Akpinar, 2010):

$$\text{Exergy efficiency} = \frac{(\text{Input Exergy} - \text{Exergy Loss})}{\text{Input Exergy}} \quad (30)$$

When drying does not take place, the exergy efficiency is 100% and gradually decreases with the onset of drying.

## 2.6 | Specific energy consumption

Since one of the main objectives of this research was to study the changes in the amount of specific energy consumed and its environmental effects, we tried to apply hybrid drying (solar-hot air) methods to the samples. The equations for calculating the specific energy consumption by a hybrid dryer (solar-hot air) in drying pennyroyal at different input air temperatures and velocities are given in the following equations (Bahammou, Tagnamas, Lamharrar, & Ildlimam, 2019; Motevali & Tabatabaei, 2017):

$$EU_{ter} = (A_{dc} \cdot U_a \cdot \rho_a \cdot C_a \cdot \Delta T \cdot 3600) \quad (31)$$

$$\rho_a = \frac{101.325}{0.287 \times T} \quad (32)$$

$$E_{mec} = E_{fan} + E_{auxiliary\ heater} \quad (33)$$

$$E_{fan} = \Delta P \cdot M_{air} \cdot t \quad (34)$$

$$E_{auxiliary\ heater} = U \cdot I \cdot t \quad (35)$$

$$SEC = \frac{EU_{(mec+ter)}}{M_W} \quad (36)$$

## 2.7 | Evaluating environmental impacts and calculating greenhouse gas emissions

Since Iran has a lot of natural gas and heavy oil, a large amount of greenhouse gases are produced in this country. All of Iran's power plants are gas-turbine, steam and combined power plants and the amount of greenhouse gas emissions from different power plants with different fuel sources are reported in Table 2. In this table, the average greenhouse gas emissions (CO<sub>2</sub>, SO<sub>2</sub>, and NO<sub>x</sub>) of Iran's power plants (gas-turbine, steam, and combined cycle) using primary fuels (natural gas and heavy oil) to produce 1 KW of energy are shown.

The total production of a power plant required for drying programs can be obtained using the following equation (Motevali & Tabatabaei, 2017):

$$\text{TotalEnergy} = \frac{SEC}{\eta_{total}} = \frac{SEC}{\eta_{Powerhouse} + \eta_{Distribution}} \quad (37)$$

## 2.8 | Experimental uncertainty analysis

Uncertainty analysis is a method used to find uncertainty in variables. During the measurement and calculation of the parameters, the uncertainties were determined using the following equation and presented in Table 3.

$$U_R = \left[ \left( \frac{\partial R}{\partial x_1} U_1 \right)^2 + \left( \frac{\partial R}{\partial x_2} U_2 \right)^2 + \dots + \left( \frac{\partial R}{\partial x_n} U_n \right)^2 \right]^{\frac{1}{2}} \quad (38)$$

**TABLE 2** Emissions of greenhouse gases and pollutants from plants using natural gas and heavy oil to produce 1 KW of energy (Nazari et al., 2010)

Power house type	Fuel type	Greenhouse gas (g/kWh)		
		NO <sub>x</sub>	SO <sub>2</sub>	CO <sub>2</sub>
Steam	Natural gas	2.69	0	636
	Heavy oil	2.52	15.28	1,025
Gas-turbine	Natural gas	1.91	0	782
	Gas oil	5.79	3.84	1,048
Combined cycle	Natural gas	2.95	0	450
	Gas oil	3.78	2.32	622

**TABLE 3** Uncertainties in measurement of parameters during drying of pennyroyal

Parameter	Unit	Value
Inlet temperature in convective dryer	°C	±0.21
Outlet temperature in convective dryer	°C	±0.21
Ambient air temperature	°C	±0.21
Drying cabinet inlet temperature	°C	±0.21
Drying cabinet outlet temperature	°C	±0.21
Drying rate	g water/(g dry solid. min)	±0.012
Time measurement	Min	±0.017
Uncertainty in the measurement of moisture quantity	g	±0.016
Uncertainty in the measurement of relative humidity of air	RH	±0.10
Uncertainty in the air velocity	m/s	±0.15
Uncertainty in mass measurement	g	±0.02
Uncertainty in moisture ratio (MR)	Dimensionless	±0.42
Uncertainty in energy utilization ratio (EUR)	Dimensionless	±0.0002
Uncertainty in energy utilization	kJ/s	±0.001
Uncertainty in exergy loss	kJ/s	±0.0001
Uncertainty in exergy efficiency	Dimensionless	±1.80
Uncertainty in specific energy consumption (SEC)	kWh/kg	±1.45

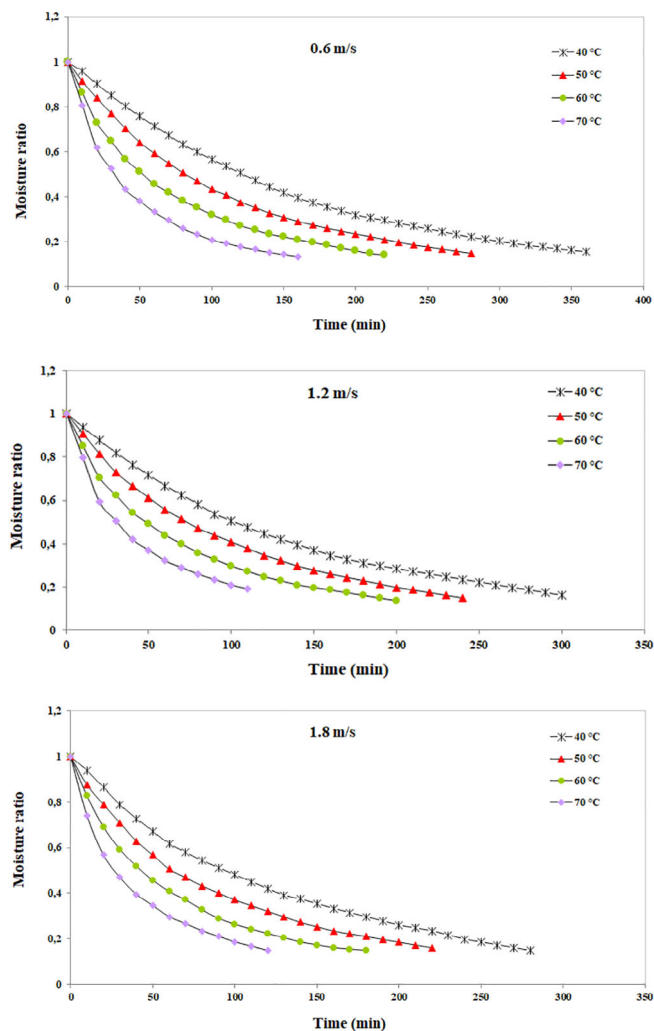
### 3 | RESULTS AND DISCUSSION

#### 3.1 | Drying kinetic

Figure 2 shows MR changes for drying pennyroyal (*Mentha pulegium*) at the temperatures of 40, 50, 60, and 70°C and the intake air speeds of 0.6, 1.2, and 1.8 m/s. It is obvious that MR constantly decreases as the drying time gets longer. This reduction in MR is more visible at higher temperatures. As the temperature rises, heat transfer and consequently the amount of moisture transfer increases (Benmakhlouf, Azzouz, Monzó Cabrera, Khdhira, & ELcfsi, 2017). Increase in the velocity of the intake air leads to increase in the moisture transfer rate, resulting in an increase in the drying rate. At higher velocities, heat transfer between solids and air occurs faster (Ghnimi et al., 2016). For example, at the speed of 1.8 m/s when the air temperature changed from 40 to 70°C, drying time dropped from 280 to 120 min. Some authors reported similar results for other agricultural products such as bay laurel leaves (Ghnimi et al., 2016), mushroom (Ghanbarian, Dastjerdi, & Torke Harchegani, 2016), and Moroccan sweet cherries (Ouaabou et al., 2018).

#### 3.2 | Drying rate

Drying rate constantly decreases as the MR is reduced or drying time increased (Figure 3). This shows that drying rate is a strong function

**FIGURE 2** Moisture ratio of pennyroyal at several conditions

of temperature, air velocity, and time. The highest rate of drying for pennyroyal occurs at the first hour of the drying process at all temperatures and the rate decreases by the passage of time. The internal resistance of the pennyroyal moisture is low at the beginning of the drying process. So, moisture will easily reach the surface and the drying rate increases (Boutelba, Glouannec, Youcef-ali, Magueresse, & Kimouche, 2019). These results are consistent with the findings of the previous researchers Wang et al. (2018) for mango in a solar-convection dryer, Koukouch et al. (2017) for olive pomace in a solar-convection dryer and Tham et al. (2017) for Java tea and sabah snake grass in a solar dryer with integrated heat pump.

#### 3.3 | Modeling

The results of MR against drying time with 14 models for thin layer drying are shown in Table 4. The best model based on RMSE,  $\chi^2$ , and  $R^2$  was specified. The results showed that the Midilli et al. model had the highest correlation since it had the maximum coefficient of determination ( $R^2 = .9995$ ), minimum chi-square ( $\chi^2 = 0.0010$ ), and the

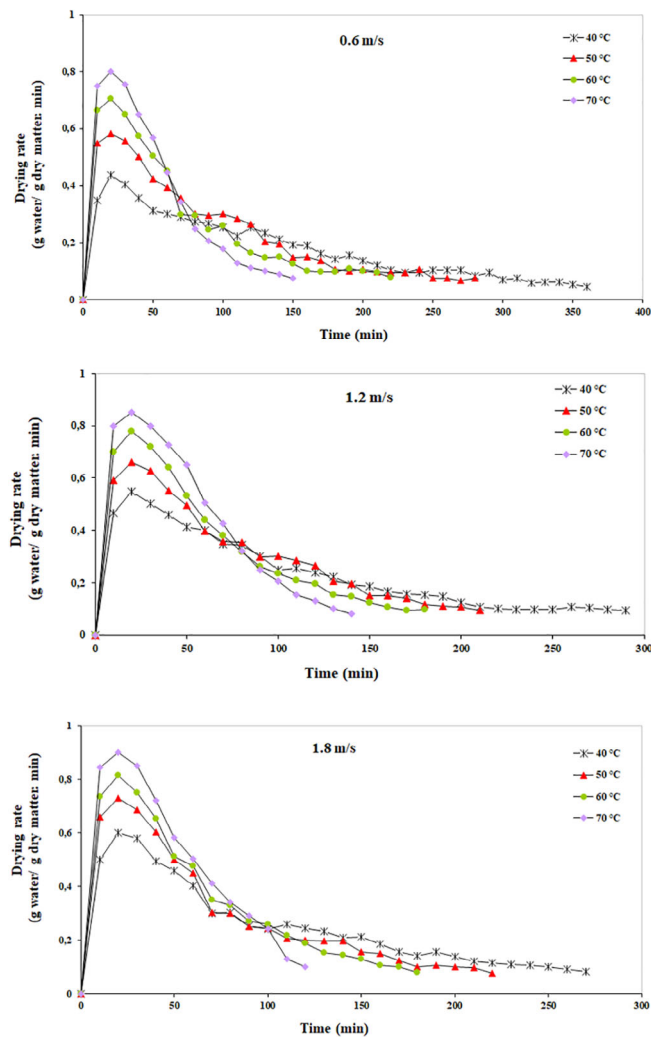


**FIGURE 3** Drying rate of pennyroyal at several conditions

lowest root mean square error (RMSE = 0.0139) for drying pennyroyal in a hybrid (solar-hot air) dryer. Therefore, the selected model can describe the pennyroyal drying behavior well. Kian-Pour and Karatas (2019) displayed that the Midilli et al. model was most suitable for describing the drying behavior of the apples. Quispe-Fuentes, Vega-Galvez, Vasquez, Uribe, and Astudillo (2017) showed that the Midilli et al. model is the best model for prediction of thin layer drying behavior of Chilean berry.

### 3.4 | Determination of $D_{\text{eff}}$

The values of  $D_{\text{eff}}$  for pennyroyal are reported in Figure 4. Effective moisture diffusion coefficient values increased as drying temperature and intake air velocity increased. The maximum effective moisture diffusion coefficient was  $2.30 \times 10^{-10} \text{ m}^2/\text{s}$  at the temperature of  $70^\circ\text{C}$  and the air velocity of 1.8 m/s. Its minimum value was  $7.92 \times 10^{-11} \text{ m}^2/\text{s}$  at the temperature of  $40^\circ\text{C}$  and the air velocity of 0.6 m/s. The  $D_{\text{eff}}$  in pennyroyal samples occurred as a result of the

**TABLE 4** Statistical comparison for the prediction of Pennyroyal's thin layer drying

Model	$R^2$	$\chi^2$	RMSE
Newton (Lewis)	0.9969	0.0077	0.0331
Page	0.9981	0.0049	0.0225
Logarithmic	0.9990	0.0021	0.0169
Henderson and Pabis	0.9973	0.0069	0.0289
Modified Henderson and Pabis	0.9962	0.0092	0.0385
Two-term	0.9963	0.0089	0.0376
Two-term exponential	0.9959	0.0098	0.0449
<b>Midilli et al.</b>	<b>0.9995</b>	<b>0.0010</b>	<b>0.0139</b>
Verma et al.	0.9985	0.0033	0.0187
Wang and Singh	0.9951	0.0119	0.0513
Approximation of diffusion	0.9945	0.0137	0.0567
Demir et al.	0.9984	0.0036	0.0193
Logistic	0.9993	0.0014	0.0151
Parabolic	0.9937	0.0157	0.0603

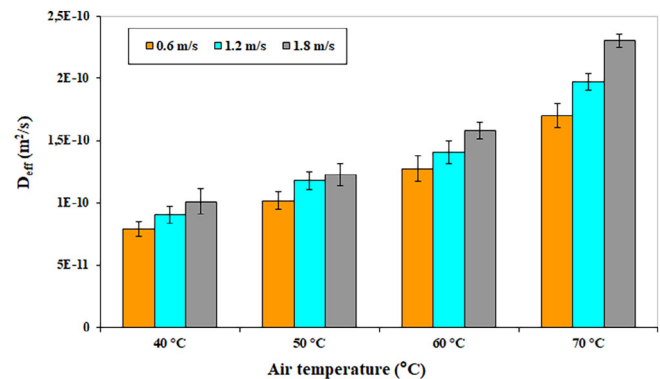


**FIGURE 4** Variation of effective moisture diffusivity with drying air velocity and air temperature

destruction of the cell wall due to increase in the temperature and velocity of the intake air, as well as decrease in moisture resistance inside the product (Tham et al., 2017). In addition,  $D_{\text{eff}}$  values for food were in the range of  $10^{-12}$  to  $10^{-8} \text{ m}^2/\text{s}$  (Das & Arora, 2018). This type of variation has been confirmed by several researchers (Adedeji, Suhr, Bhadriraju, & Alavi, 2017; Aktas, Sevik, Amini, & Khanlari, 2016; Sehwat et al., 2018; Taghinezhad et al., 2020).

### 3.5 | Activation energy

For different temperatures and velocities of the intake air, the activation energy values for pennyroyal in the hybrid dryer were 22.41–25.18 kJ/mol. These results are shown in Table 5. Kian-Pour and Karatas (2019) reported the  $E_a$  of apple slices with different temperatures in the range of 20.41–36.51 kJ/mol. In their work, Quispe-Fuentes et al. (2017) reported the  $E_a$  of Chilean berry dried in a convective dryer at 40, 50, 60, and  $70^\circ\text{C}$  and air velocity 2 m/s was 42 kJ/mol.

**TABLE 5** Activation energy values and the related correlation coefficients for pennyroyal

Parameter	0.6 m/s	1.2 m/s	1.8 m/s
Activation energy ( $E_a$ ) (kJ/mol)	22.41	23.77	25.18
Coefficient of determination ( $R^2$ )	0.9952	0.9818	0.9689

### 3.6 | Energy utilization ratio

Various experiments were carried out to calculate the energy utilization ratio (EUR) at different temperatures and velocities of the intake air for drying pennyroyal and the results were shown in Figure 5. As can be seen, the EUR at different temperatures and velocities of the intake air was within the range of 0.056–0.957 for pennyroyal. The maximum amount of energy consumed was 0.957 at the air temperature of 70°C and the air velocity of 1.8 m/s and the lowest amount was 0.056 at air temperature of 40°C and the air velocity of 0.6 m/s.

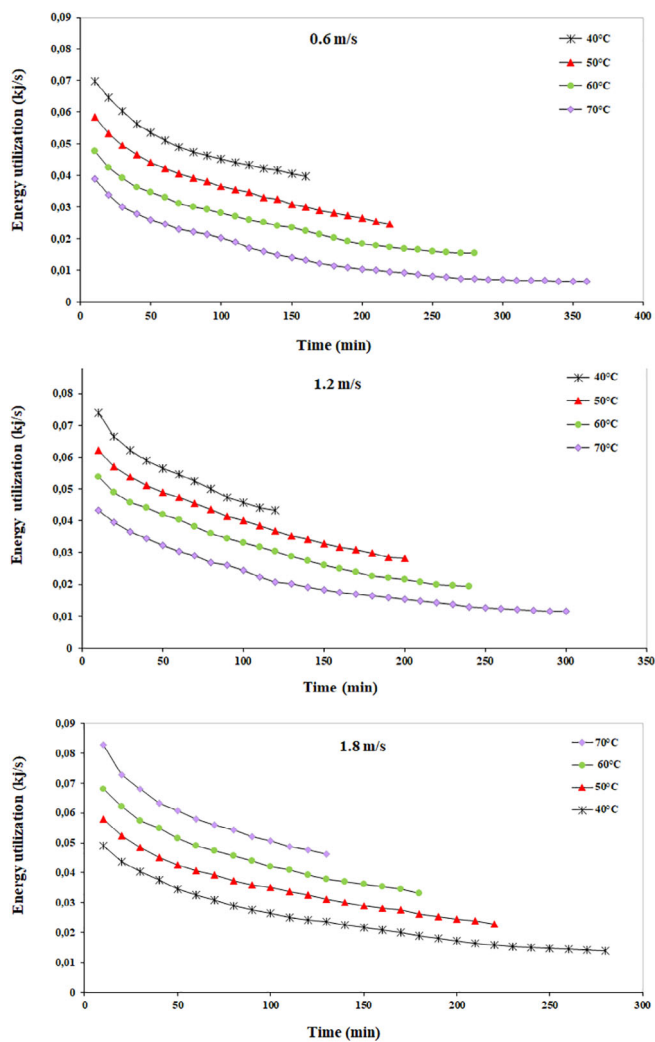
#### 3.6.1 | Effect of air temperature on EUR

Pennyroyal drying experiments were conducted at different temperatures between 40 and 70°C and different air velocities and the results were presented in Figure 5. The results show that the EUR increases as the temperature of the dryer wall increases from 40 to 70°C. The highest level of energy consumption is observed at the beginning of the pennyroyal drying period, and then its amount decreases with the passage of time. According to Equation (24), the reduction of EUR over time is quite reasonable.

The EUR in the hybrid (solar-hot air) dryer increases as the air temperature rises. Increase in the temperature of the dryer leads to increase in the rate of moisture evaporation from the product. In other words, at high temperatures, heat, and mass transfer are high and the loss of moisture is excessive (Motevali, Jafari, & Hashemi, 2018). These results are similar to those reported for drying mushrooms in the fluid bed dryer (Darvishi et al., 2018), drying carrots in the fluid bed dryer (Nazghelichi et al., 2010), and drying rice in the fluidized bed dryer (Sarker, Ibrahim, Abdul Aziz, & Punan, 2015).

#### 3.6.2 | Effect of air velocity on EUR

Intake air velocities for pennyroyal drying experiments ranged from 0.6 to 1.8 m/s. The experiments were carried out at different intake air temperatures and the results were reported in Figure 5. The results show that energy utilization ratio increases as the air velocity rises and decreases by the passage of time. Increase in air velocity increases energy utilization and the evaporation of the moisture content from the product surface (Azadbakht et al., 2018). These results are similar to those reported by researchers for drying potatoes

**FIGURE 5** Effect air temperature and air velocity on energy utilization ratio

(Azadbakht, Aghili, Ziaratban, & Torshizi, 2017) and Kodo millet grains (Yogendrasasidhar & Setty, 2018).

### 3.7 | Energy utilization

Figure 6 shows the energy utilization (EU) value for the two parameters of temperature and air velocity. The maximum EU was 0.0826 kJ/s at the temperature of 70°C and the air velocity of 1.8 m/s and the lowest EU was 0.0064 kJ/s at 40°C and the air speed of 0.6 m/s.

#### 3.7.1 | Effect of air temperature on EU

The results shown in Figure 6 indicate that by increasing the air temperature, EU increases. It can be noted that the input enthalpy has increased with increasing temperature and the amount of intake air, which leads to increased energy consumption. In addition, due to the

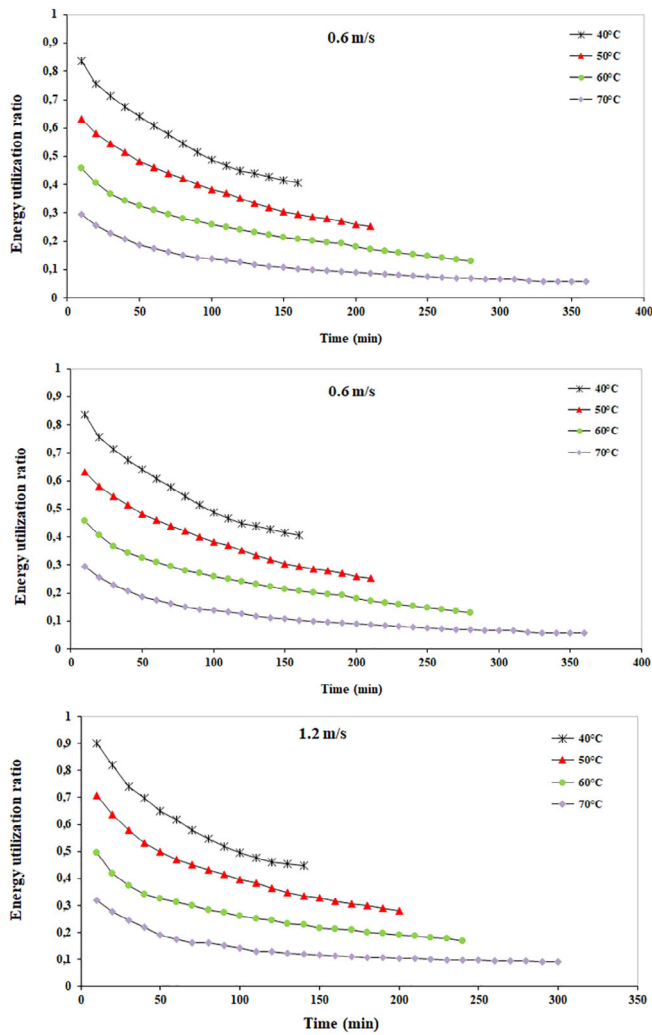


**FIGURE 6** Effect air temperature and air velocity on energy utilization (kJ/s)

direct relationship between energy consumption and EU, energy utilization increases. In similar studies conducted on drying eggplants in a fluidized bed dryer (Azadbakht, Torshizi, Ziaratban, & Aghili, 2017), drying cassava starch in a tray dryer (Aviara, Onuoha, Falola, & Igbeka, 2017), and drying coroba slices in a convective dryer (Corzo et al., 2008), the researchers reported that energy utilization increased as the intake air temperature increased.

### 3.7.2 | Effect of air velocity on EU

The results illustrated in Figure 6 show that by increasing air velocity, energy utilization increases. According to Equation (13), the amount of EU depends on the mass flow of the air. Therefore, when air velocity increases, the mass flow increases and leads to increased energy utilization (Yogendrasidhar & Setty, 2018). These results are in line with the findings of Azadbakht, Torshizi, et al. (2017) in their study of drying potatoes and Motevali and Minaee (2012) on drying pomegranates.

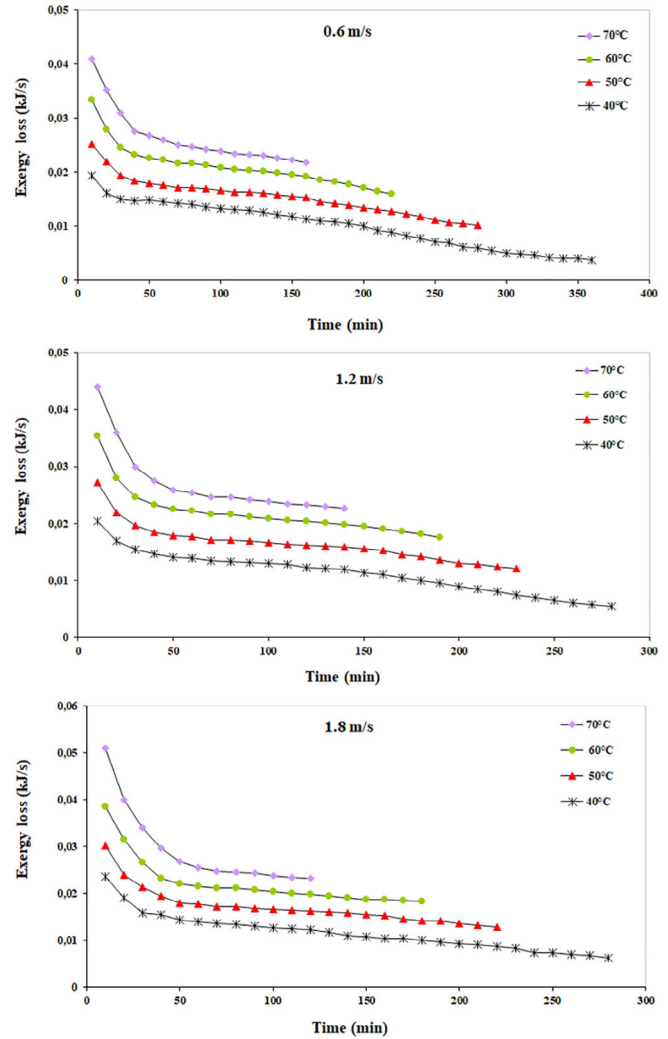


**FIGURE 7** Effect of air temperature and air velocity on exergy loss (kJ/s)

## 3.8 | Exergy loss (kJ/s)

Figure 7 shows the amount of exergy loss for the two parameters of intake air temperature and velocity. The highest exergy loss was approximately 0.051 kJ/s, which occurred at the temperature of 70°C, and the air velocity of 1.8 m/s. The lowest exergy loss was 0.0037 kJ/s at 40°C temperature and 0.6 m/s air velocity.

### 3.8.1 | Effect of air temperature on exergy loss (kJ/s)

Exergy loss is the difference between the dryer's input exergy and its output exergy. Input exergy is based on the dryer's wall temperature (Equation (27)) and output exergy is based upon the output air temperature (Equation (28)). Figure 7 shows that by increasing the intake air temperature, the amount of exergy loss increases. Exergy loss is higher in the initial drying phase. In addition, the loss of exergy decreases steadily over time since the passage of time

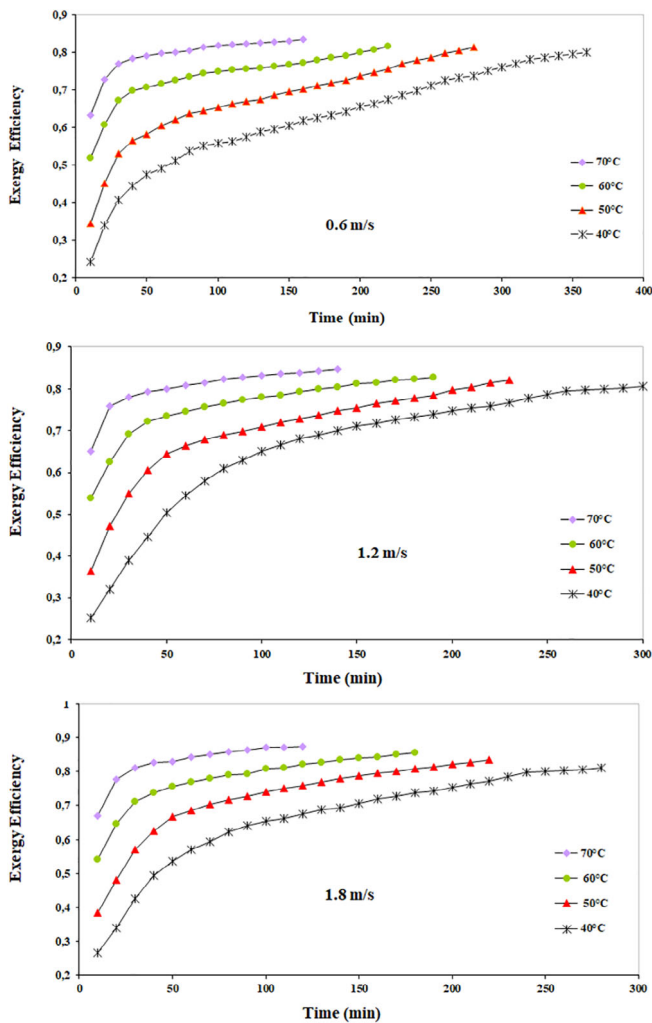


**FIGURE 8** Effect of air temperature and air velocity on exergy efficiency

reduces the moisture content in the pennyroyals. A lower amount of moisture has a lower capacity to absorb exergy, so the exhaust air has a lower exergy than the intake air (Azadbakht, Torshizi, et al., 2017; Darvishi et al., 2018). Higher drying temperatures have higher exergy and this exergy reduces the product's moisture or exergy consumption and thus increases exergy loss (Corzo et al., 2008).

### 3.8.2 | Effect of air velocity on exergy loss (kJ/s)

As the intake air velocity increases, the exergy loss increases too, resulting in a mass transfer rate that decreases the pennyroyal's moisture content. The drying process time also decreases and less energy is transferred to the outside of the dryer chamber. So, the output exergy increases (Aghbashlo et al., 2008; Akpınar et al., 2006). In similar investigations, the researchers reported that with increasing inlet air velocity, the exergy loss increases (Beigi, Tohidi, & Torshizi, 2017; Darvishi et al., 2018).

**TABLE 6** Specific energy consumption during the drying of pennyroyal by a hybrid (solar-hot air) dryer

Air velocity (m/s)	Temperatures (°C)	SEC (kWh/kg)
0.6	40	60.48
	50	41.85
	60	36.40
	70	32.20
1.2	40	42.20
	50	37.43
	60	31.41
	70	25.22
1.8	40	29.28
	50	23.47
	60	22.40
	70	14.11

### 3.9 | Exergy efficiency

The exergy efficiency curves are shown in Figure 8 with regard to the temperature and velocity of the intake air for the dried pennyroyal. The maximum exergy efficiency was 0.8731 at the temperature of 70°C and the air velocity of 1.8 m/s. The minimum exergy efficiency was 0.2428 at the air temperature of 40°C and the air velocity of 0.6 m/s.

#### 3.9.1 | Effect of air temperature on exergy efficiency

Figure 8 shows that the exergy efficiency increased during the drying time. Increasing the dryer's temperature caused an increase in exergy loss, but this amount was lower than the increased exergy value. According to Equation (29), the exergy efficiency increases by increasing temperature at different velocities of the intake air. Exergy efficiency has a direct relationship with the dryer's energy efficiency. The evaporation rate of moisture and mass transfer rate increase as the intake air temperature rises. This increases the exergy efficiency of the hybrid (solar-hot air) dryer. Similar results have been reported in the drying of various products such as soybean (Ranjbaran & Zare, 2013), carrot cubes (Nazghelichi et al., 2010), and green olive (Colak & Hepbasli, 2007).

#### 3.9.2 | Effect of air velocity on exergy efficiency

Increase in the intake air velocity and the drying time increases the exergy efficiency (Figure 8), because the entropy and enthalpy of the dryer's intake air increase by the rising air velocity, which results in increased exergy efficiency. These results were similar to those of Motevali and Minaee (2012) and Nikbakht, Motevali, and Minaee (2014) for drying pomegranates. Yogendrasasidhar and

**TABLE 7** GHG emissions from different power plants while using a hybrid (solar-hot air) dryer for drying pennyroyal

Power plants	GHG	0.6 m/s						1.2 m/s						1.8 m/s																				
		40 °C		60 °C		70 °C		40 °C		60 °C		70 °C		40 °C		60 °C		70 °C																
		CO <sub>2</sub>	SO <sub>2</sub>	NOx																														
Steam power— natural gas	GHG	30,915.81	0	143.88	26,617.51	0	123.88	20,483.65	0	95.33	23,810.73	0	110.81	26,844.16	0	124.93	16,041.96	0	74.66	19,978.82	0	92.98	18,622.08	0	86.69	14,926.92	0	69.47	14,249.23	0	66.31	8,979.34	0	41.79
	CO <sub>2</sub>	30,915.81	0	143.88	26,617.51	0	123.88	20,483.65	0	95.33	23,810.73	0	110.81	26,844.16	0	124.93	16,041.96	0	74.66	19,978.82	0	92.98	18,622.08	0	86.69	14,926.92	0	69.47	14,249.23	0	66.31	8,979.34	0	41.79
	SO <sub>2</sub>	0	0	0	0	0	0	0	0	0	0	0	0	0	0	0	0	0	0	0	0	0	0	0	0	0	0	0	0	0	0	0	0	0
Steam power— heavy oil	GHG	49,825	742.75	122.49	42,897.71	639.48	105.46	37,317.83	556.30	91.74	33,012.17	492.12	81.16	43,262.99	644.93	106.36	38,374.21	572.05	94.34	32,198.57	479.99	79.16	30,012	447.53	73.80	24,058.12	358.64	59.14	22,964.57	342.34	56.45	14,471.43	215.73	35.57
	CO <sub>2</sub>	49,825	742.75	122.49	42,897.71	639.48	105.46	37,317.83	556.30	91.74	33,012.17	492.12	81.16	43,262.99	644.93	106.36	38,374.21	572.05	94.34	32,198.57	479.99	79.16	30,012	447.53	73.80	24,058.12	358.64	59.14	22,964.57	342.34	56.45	14,471.43	215.73	35.57
	SO <sub>2</sub>	742.75	122.49	0	639.48	105.46	0	556.30	91.74	0	492.12	81.16	0	644.93	106.36	0	572.05	94.34	0	479.99	79.16	0	447.53	73.80	0	358.64	59.14	0	342.34	56.45	0	215.73	35.57	0
Gas turbine— natural gas	GHG	38,012.83	0	92.84	32,727.81	79.93	105.46	28,470.77	0	69.53	25,185.87	0	80.61	33,006.49	0	71.50	29,276.71	0	80.61	24,565.15	59.99	48.17	22,896.96	55.94	44.83	18,354.58	44.83	42.79	17,520.28	42.79	26.96	11,040.64	0	0
	CO <sub>2</sub>	38,012.83	0	92.84	32,727.81	79.93	105.46	28,470.77	0	69.53	25,185.87	0	80.61	33,006.49	0	71.50	29,276.71	0	80.61	24,565.15	59.99	48.17	22,896.96	55.94	44.83	18,354.58	44.83	42.79	17,520.28	42.79	26.96	11,040.64	0	0
	SO <sub>2</sub>	0	0	0	0	0	0	0	0	0	0	0	0	0	0	0	0	0	0	0	0	0	0	0	0	0	0	0	0	0	0	0	0	0
Gas turbine—gas oil	GHG	50,943.03	186.66	281.45	43,860.29	160.70	242.31	38,155.2	139.80	210.80	33,752.93	123.67	162.07	44,233.77	244.38	189.93	39,235.29	143.76	216.76	32,921.08	120.62	181.88	30,685.44	112.46	90.12	24,597.96	86.03	129.72	23,479.87	86.03	54.21	14,796.15	54.21	81.74
	CO <sub>2</sub>	50,943.03	186.66	281.45	43,860.29	160.70	242.31	38,155.2	139.80	210.80	33,752.93	123.67	162.07	44,233.77	244.38	189.93	39,235.29	143.76	216.76	32,921.08	120.62	181.88	30,685.44	112.46	90.12	24,597.96	86.03	129.72	23,479.87	86.03	54.21	14,796.15	54.21	81.74
	SO <sub>2</sub>	186.66	281.45	0	160.70	242.31	0	139.80	210.80	0	123.67	162.07	0	244.38	189.93	143.76	143.76	216.76	0	120.62	181.88	146.04	169.58	112.46	90.12	24,597.96	86.03	129.72	23,479.87	86.03	54.21	14,796.15	54.21	81.74
Combine cycle— natural gas	GHG	21,874.39	0	143.39	18,833.14	123.46	158.19	16,383.44	0	107.40	14,493.15	0	124.51	18,993.51	0	110.44	16,847.21	0	110.44	14,135.96	92.66	74.40	13,176	86.40	69.24	10,562.1	69.24	66.09	8,781.687	66.09	41.64	4,164	0	0
	CO <sub>2</sub>	21,874.39	0	143.39	18,833.14	123.46	158.19	16,383.44	0	107.40	14,493.15	0	124.51	18,993.51	0	110.44	16,847.21	0	110.44	14,135.96	92.66	74.40	13,176	86.40	69.24	10,562.1	69.24	66.09	8,781.687	66.09	41.64	4,164	0	0
	SO <sub>2</sub>	0	0	0	0	0	0	0	0	0	0	0	0	0	0	0	0	0	0	0	0	0	0	0	0	0	0	0	0	0	0	0	0	0
Combine cycle— turbine-gas oil	GHG	30,235.27	112.77	183.74	26,031.59	97.09	158.19	22,645.55	84.46	137.62	20,032.75	74.72	97.92	26,253.25	86.85674	72.87	23,286.59	86.85674	118.74	19,539.04	72.87	58.51	18,212.16	67.95	54.45	14,599.17	54.45	51.97	13,935.57	51.97	32.75	8,781.687	32.75	53.36
	CO <sub>2</sub>	30,235.27	112.77	183.74	26,031.59	97.09	158.19	22,645.55	84.46	137.62	20,032.75	74.72	97.92	26,253.25	86.85674	72.87	23,286.59	86.85674	118.74	19,539.04	72.87	58.51	18,212.16	67.95	54.45	14,599.17	54.45	51.97	13,935.57	51.97	32.75	8,781.687	32.75	53.36
	SO <sub>2</sub>	112.77	183.74	0	97.09	158.19	0	84.46	137.62	0	74.72	97.92	0	79.92	86.85674	72.87	23,286.59	86.85674	118.74	19,539.04	72.87	58.51	18,212.16	67.95	54.45	14,599.17	54.45	51.97	13,935.57	51.97	32.75	8,781.687	32.75	53.36

Setty (2018) reported that the exergy efficiency increased (approximately from 0.78 to 0.94 for Kodo millet) by raising the air velocity from 1.01 to 1.7 m/s and the air temperature from 40 to 60°C.

### 3.10 | Specific energy consumption

Table 6 represents the SEC of the entire drying process for pennyroyal in a hybrid (solar-hot air) dryer. The maximum amount of energy consumed was 48.60 kWh/kg at the intake air temperature of 40°C and the intake air velocity of 0.6 m/s. The minimum amount of energy consumed was 14.11 kWh/kg at the intake air temperature of 70°C and the air velocity of 1.8 m/s. Moreover, the specific energy consumption increased as the air velocity and temperature decreased. Increase in the intake air temperature and velocity resulted in the rapid transfer of mass and increase in the speed of moisture transfer from the surface of the product. So, the amount of specific energy consumption decreased (Kaveh et al., 2018). These findings are in agreement with the documented values of 23.45–10.55 kWh/kg applied for mint leaves in a convective dryer (Beigi, 2019) and 227.39 to 337.79 kWh/kg for a convective hot air dryer of sweet potato slices (Onwude, Hashim, Abdan, Janius, & Chen, 2018).

### 3.11 | Greenhouse gases

Table 7 shows that the highest CO<sub>2</sub> level (116,516.6 g) occurred at 40°C and 0.6 m/s for the gas turbine-gas oil plant while its lowest level (12,721.5 g) occurred at the temperature of 70°C and the air velocity of 1.8 m/s for the combined cycle-natural gas plant. In addition, SO<sub>2</sub> increased by decrease in the temperature and the air flow rate and reached the highest level at the temperature of 40°C and the air velocity of 0.6 m/s. The analysis of NO<sub>x</sub> changes showed that its variation is inversely related to temperature and air flow velocity. The highest amount of NO<sub>x</sub> (643.73 g) was produced at 40°C and the air velocity of 0.6 m/s at the gas turbine-gas oil plant. Its lowest level was 53.99 g at the temperature of 70°C and the air velocity of 1.8 m/s at the gas turbine-natural gas plant. The high emission of greenhouse gases in a hybrid (solar-hot air) dryer as a result of increase in temperature reduces energy consumption in the unit of time. At low temperatures, it leads to increased greenhouse gas emissions. Solar collectors improve the absorption of heat from the sun, which in turn increases air temperature and reduces energy consumption and greenhouse gas emissions (Ziaforoughi & Esfahani, 2016). Tripathy (2015) reported the CO<sub>2</sub> for drying potato slice using a solar dryer. The amounts of CO<sub>2</sub> in three coal-fired, light diesel oil and natural gas plants for potato slices were  $1.44 \times 10^4$ ,  $9.47 \times 10^3$ , and  $4.74 \times 10^3$  tons, respectively. Motevali and Tabatabaei (2017) showed that the lowest amounts of greenhouse gases (CO<sub>2</sub>, SO<sub>2</sub>, and NO<sub>x</sub>) were obtained in the combination of solar-hot air at the highest air temperature. They also got the highest amounts of CO<sub>2</sub> (11,994.78 g), SO<sub>2</sub> (170 g), and NO<sub>x</sub> (66.26 g) at the lowest air temperature. Kaveh, Amiri Chayjan,

Taghinezhad, Rasooli Sharabiani, and Motevali (2020) also obtained similar results.

## 4 | CONCLUSION

Experiments for drying pennyroyal using a hybrid (solar-hot air) dryer were carried out to evaluate the drying behavior of pennyroyal under different parameters (temperature and air velocity). The effects of intake air temperature and intake air velocity on drying kinetics, effective moisture diffusion, energy utilization ratio, energy utilization, exergy loss, exergy efficiency, specific energy consumption, and greenhouse gas emissions in the process of drying pennyroyal plant were examined.

- Increase in the intake air temperature and velocity resulted in decrease in the drying time.
- Midilli et al's model was selected as the best model for the prediction of pennyroyal MR.
- Effective moisture diffusion coefficient for pennyroyal was between  $7.92 \times 10^{-11}$  m<sup>2</sup>/s and  $2.30 \times 10^{-10}$  m<sup>2</sup>/s.
- The EUR increased by increasing the intake air temperature and air velocity.
- The highest and lowest EU rates were 0.0826 kJ/s and 0.0064 kJ/s, respectively.
- Increasing the intake air temperature and velocity increased the exergy loss.
- Exergy efficiency increased with increasing intake air temperature and air velocity.
- The highest (48.60 kWh/kg) and lowest (14.11 kWh/kg) amounts of specific energy consumption were obtained.
- In the process of drying pennyroyal, increase in the intake air temperature caused the reduction of GHG. Low levels of GHG occurred at high drying temperatures. Increasing the temperature and airflow rate resulted in a significant reduction in GHG.

## NOMENCLATURE

$A_{def}$	surface in contact with the dryer's body (m <sup>2</sup> )
$A_{dc}$	cross section of the drying chamber (m <sup>2</sup> )
$C_a$	input or output air specific heat (kJ/kg°C)
$C_p$	specific heat of the input or output product (kJ/kg°C)
$C$	specific heat of the input or output air and the input or output product (kJ/kg°C)
$C_{ai}$	specific heat of the input air (kJ/kg°C)
$D_{eff}$	effective moisture diffusivity (m <sup>2</sup> /s)
$DR$	drying rate
$D_0$	intercept that is constant
$EU$	amount of the energy used (kJ/s)
$E_a$	activation energy (kJ/mol)
$Ex$	exergy of the air or the input or output product (kJ/s)
$Ex_{pf}$	exergy of the fresh product (kJ/s)
$Ex_{ao}$	output air exergy (kJ/s)

$EX_{ai}$	input air exergy (kJ/s)
$EX_{PD}$	exergy of the output product (dried product) (kJ/s)
$EX_{deff}$	exergy rate of the dryer's body (kJ/s)
$h_{ai}$	input air enthalpy (kJ/kg)
$h_{PF}$	enthalpy of the input fresh product (kJ/kg)
$h_{ao}$	output air enthalpy (kJ/kg)
$h_{PD}$	dry product's enthalpy (kJ/kg)
$h_a$	input or output air enthalpy (kJ/kg)
$h_p$	input or output product enthalpy (kJ/kg)
$h_{fg}$	latent heat of vaporization of water (kJ/kg)
$I$	current (A)
$L$	half the thickness of each sample
$MC_{db}$	moisture content
$M_t$	moisture content (% d.b.)
$M_o$	initial moisture content (% d.b.)
$M_e$	equilibrium moisture content (% d.b.)
$MR$	moisture ratio (decimal)
$MR_{expi}$	stands for the experimental values
$MR_{prei}$	predicted values by calculating from the model for this measurements
$MC_{t+\Delta t}$	moisture content at $t + \Delta t$
$\dot{m}_{PF}$	rate of the fresh product flow (kg/s)
$\dot{m}_{ai}$	input air flow rate (kg/s)
$\dot{m}_{ao}$	output air flow rate (kg/s)
$m_a$	air flow rate (kg/s)
$\dot{m}_{PD}$	dry product's flow rate (kg/s)
$MW$	mass transfer amount (kg)
$m$	mass flow rate of the air or the input or output product (kg/s)
$n$	number of terms taken into consideration
$N$	number of observations
$P$	equivalent of the air pressure of the environment equal to $101 \times 103$ Pa
$\dot{Q}_{deff}$	heat loss rate from the dry body (kJ/s).
$\dot{Q}_{aol}$	heat dissipated from the output air (kJ/s)
$\dot{Q}_{evap}$	evaporated heat (kg/s)
$R_g$	universal gas constant (equal to 8.3143 kJ/mol)
$SEC$	specific energy consumption
$T_a$	inlet or outlet air temperature ( $^{\circ}\text{C}$ )
$T_{\infty}$	ambient temperature ( $^{\circ}\text{C}$ )
$T_P$	input or output product's temperature ( $^{\circ}\text{C}$ )
$T_{mvdef}$	average temperature of the dryer's body (at three points) ( $^{\circ}\text{C}$ )
$T_{ai}$	input air temperature ( $^{\circ}\text{C}$ )
$T_{ao}$	output air temperature ( $^{\circ}\text{C}$ )
$t$	drying time (s)
$T_{abs}$	temperature inside the drying chamber ( $^{\circ}\text{K}$ )
$U_{def}$	thermal loss factor of the dryer body ( $\text{Kw}/\text{m}^2\text{C}$ )
$U$	voltage (V)
$U_a$	input air velocity (m/s)
$w$	absolute humidity of the input or output air
$W_i$	plant's weight during drying
$W_d$	weight of the dried plant

$z$  number of constants, respectively

$\sum EX_l$  sum of the exergy loss (kJ/s)

$\sum EX_i$  sum of the input exergy (kJ/s)

$\sum EX_o$  sum of the output exergy (kJ/s)

$\rho_a$  air density ( $\text{kg}/\text{m}^3$ )

## CONFLICT OF INTEREST

The authors have declared no conflicts of interest for this article.

## DATA AVAILABILITY

The data that support the findings of this study are available from the corresponding author upon reasonable request.

## ETHICS STATEMENT

Ethics approval was not required for this research.

## ORCID

Mohammad Kaveh  <https://orcid.org/0000-0001-5285-2211>

Hamed Karami  <https://orcid.org/0000-0002-0654-6149>

Ahmad Jahanbakhshi  <https://orcid.org/0000-0003-1944-3090>

## REFERENCES

- Abbaspour-Gilandeh, Y., Jahanbakhshi, A., & Kaveh, M. (2020). Prediction kinetic, energy and exergy of quince under hot air dryer using ANNs and ANFIS. *Food Science & Nutrition*, 8(1), 594–611. <https://doi.org/10.1002/fsn3.1347>
- Abbaspour-Gilandeh, Y., Kaveh, M., & Jahanbakhshi, A. (2019). The effect of microwave and convective dryer with ultrasound pre-treatment on drying and quality properties of walnut kernel. *Journal of Food Processing and Preservation*, 43(11), e14178. <https://doi.org/10.1111/jfpp.14178>
- Adedeji, A. A., Suhr, E., Bhadriraju, S., & Alavi, S. (2017). Drying characteristics of bean analog – A sorghum based extruded product. *Journal of Food Processing and Preservation*, 41(2), e12856. <https://doi.org/10.1111/jfpp.12856>
- Aghbashlo, M., Kianmehr, M., & Arabhosseini, A. (2008). Energy and exergy analyses of thin-layer drying of potato slices in a semi-industrial continuous band dryer. *Drying Technology*, 26, 1501–1508. <https://doi.org/10.1080/07373930802412231>
- Ahmadi, M., Rozkosh, M., & Haghighifard, N. J. (2014). Emission evaluation of CO<sub>2</sub> and CH<sub>4</sub> gases in the selected gas pressure booster station in the Bangestan field of the National Iranian oil Company. *Environmental Health Engineering and Management Journal*, 1(1), 29–35. <https://ssrn.com/abstract=2610033>
- Akpinar, E. K. (2010). Drying of mint leaves in a solar dryer and under open sun: Modelling, performance analyses. *Energy Conversion and Management*, 51, 2407–2418. <https://doi.org/10.1016/j.enconman.2010.05.005>
- Akpinar, E. K., Midilli, A., & Bicer, Y. (2006). The first and second law analyses of thermodynamic of pumpkin drying process. *Journal of Food Engineering*, 72(4), 320–331. <https://doi.org/10.1016/j.jfoodeng.2004.12.011>
- Aktas, M., Khanlari, A., Amini, A., & Sevik, S. (2017). Performance analysis of heat pump and infrared-heat pump drying of grated carrot using energy-exergy methodology. *Energy Conversion and Management*, 132, 327–338. <https://doi.org/10.1016/j.enconman.2016.11.027>
- Aktas, M., Sevik, S., Amini, A., & Khanlari, A. (2016). Analysis of drying of melon in a solar-heat recovery assisted infrared dryer. *Solar Energy*, 137, 500–515. <https://doi.org/10.1016/j.solener.2016.08.036>

- Atalay, H., Çoban, M. T., & Kincay, O. (2017). Modeling of the drying process of apple slices: Application with a solar dryer and the thermal energy storage system. *Energy*, 134, 382–391. <https://doi.org/10.1016/j.energy.2017.06.030>
- Aviara, N. A., Onuoha, L. N., Falola, O. E., & Igbeka, J. (2017). Energy and exergy analyses of native cassava starch drying in a tray dryer. *Energy*, 73, 809–817. <https://doi.org/10.1016/j.energy.2014.06.087>
- Azadbakht, M., Aghili, H., Ziaratban, A., & Torshizi, M. V. (2017). Application of artificial neural network method to exergy and energy analyses of fluidized bed dryer for potato cubes. *Energy*, 120, 947–958. <https://doi.org/10.1016/j.energy.2016.12.006>
- Azadbakht, M., Torshizi, M., Noshad, F., & Rokhbin, A. (2018). Application of artificial neural network method for prediction of osmotic pretreatment based on the energy and exergy analyses in microwave drying of orange slices. *Energy*, 165, 836–845. <https://doi.org/10.1016/j.energy.2018.10.017>
- Azadbakht, M., Torshizi, M., Ziaratban, A., & Aghili, H. (2017). Energy and exergy analyses during eggplant drying in a fluidized bed dryer. *Agricultural Engineering International: The CIGR e-journal*, 19(3), 177–182. <https://cigrjournal.org/index.php/Ejournal/article/view/4116>
- Badaoui, O., Hanini, S., Djebli, A., Brahim, H., & Benhamou, A. (2019). Experimental and modeling study of tomato pomace waste drying in a new solar greenhouse: Evaluation of new drying models. *Renewable Energy*, 133, 144–155. <https://doi.org/10.1016/j.renene.2018.10.020>
- Bahammou, Y., Tagnamas, Z., Lamharrar, A., & Idlimam, A. (2019). Thin-layer solar drying characteristics of Moroccan horehound leaves (*Marubium vulgare* L.) under natural and forced convection solar drying. *Solar Energy*, 188, 958–969. <https://doi.org/10.1016/j.solener.2019.07.003>
- Beigi, M. (2019). Drying of mint leaves: Influence of the process temperature on dehydration parameters, quality attributes, and energy consumption. *Journal of Agricultural Science Technology*, 21, 77–88. <https://jast.modares.ac.ir/article-23-16067-en.html>
- Beigi, M., Tohidi, M., & Torki-Harchegani, M. (2017). Exergetic analysis of deep-bed drying of rough rice in a convective dryer. *Energy*, 140, 374–382. <https://doi.org/10.1016/j.energy.2017.08.100>
- Benmakhlof, N., Azzouz, S., Monzó Cabrera, J., Khdhira, H., & ElCafsi, A. (2017). Controlling mechanisms of moisture diffusion in convective drying of leather. *Heat and Mass Transfer*, 53(4), 1237–1245. <https://doi.org/10.1007/s00231-016-1900-8>
- Boutelba, I. Z. S., Glouannec, P., Youcef-ali, S., Magueresse, A., & Kimouche, N. (2019). Thermo-hydrous behavior of dried un-blanchéd potato samples. *Journal of Food Engineering*, 240, 160–170. <https://doi.org/10.1016/j.jfoodeng.2018.07.027>
- Colak, N., & Hepbasli, A. (2007). Performance analysis of drying of green olive in a tray dryer. *Journal of Food Engineering*, 80(4), 1188–1193. <https://doi.org/10.1016/j.jfoodeng.2006.09.017>
- Corzo, O., Bracho, N., Vasquez, A., & Pereira, A. (2008). Energy and exergy analyses of thin layer drying of coroba slices. *Journal of Food Engineering*, 86, 151–161. <https://doi.org/10.1016/j.jfoodeng.2007.05.008>
- Darvishi, H., Azadbakht, M., & Noralahi, B. (2018). Experimental performance of mushroom fluidized-bed drying: Effect of osmotic pretreatment and air recirculation. *Renewable Energy*, 120, 201–208. <https://doi.org/10.1016/j.renene.2017.12.068>
- Das, I., & Arora, A. (2018). Alternate microwave and convective hot air application for rapid mushroom drying. *Journal of Food Engineering*, 223, 208–219. <https://doi.org/10.1016/j.jfoodeng.2017.10.018>
- Ergün, A., Ceylan, I., Acar, B., & Erkaymaz, O. (2017). Energy-exergy-Ann analyses of solar-assisted fluidized bed dryer. *Drying Technology*, 35(4), 1711–1720. <https://doi.org/10.1080/07373937.2016.1271338>
- Fudholi, A., Sopian, K., Othman, M. Y., & Ruslan, M. H. (2014). Energy and exergy analyses of solar drying system of red seaweed. *Energy and Buildings*, 68, 121–129. <https://doi.org/10.1016/j.enbuild.2013.07.072>
- Ghanbarian, D., Dastjerdi, M. B., & Torki Harchegani, M. (2016). Mass transfer characteristics of bisporus mushroom (*Agaricus bisporus*) slices during convective hot air drying. *Heat and Mass Transfer*, 52(5), 1081–1088. <https://doi.org/10.1007/s00231-015-1629-9>
- Ghnimi, T., Hassini, L., & Bagane, M. (2016). Experimental study of water desorption isotherms and thin layer convective drying kinetics of bay laurel leaves. *Heat and Mass Transfer*, 52(12), 2649–2659. <https://doi.org/10.1007/s00231-016-1770-0>
- Hassanpouraghdam, M. B., & Hassani, A. (2014). Oven and conventional drying methods affect volatile oil content and composition of *Mentha pulegium* L. *Journal of Essential Oil Bearing Plants*, 17(2), 346–352. <https://doi.org/10.1080/0972060X.2014.895152>
- Jahanbakhshi, A., Kaveh, M., Taghinezhad, E., & Sharabiani, V. R. (2020). Assessment of kinetics, effective moisture diffusivity, specific energy consumption, shrinkage, and color in the pistachio kernel drying process in microwave drying with ultrasonic pretreatment. *Journal of Food Processing and Preservation*, e14449. <https://doi.org/10.1111/jfpp.14449> (In press).
- Karami, H., Kaveh, M., Mirzaee-Ghaleh, E., & Taghinezhad, E. (2018). Using PSO and GWO techniques for prediction some drying properties of tarragon (*Artemisia dracunculus* L.). *Journal of Food Process Engineering*, 41(8), e12921. <https://doi.org/10.1111/jfpe.12921>
- Karami, H., Rasekh, M., Darvishi, Y., & Khaledi, R. (2017). Effect of drying temperature and air velocity on the essential oil content of *Mentha aquatica* L. *Journal of Essential Oil Bearing Plants*, 20(4), 1131–1136.
- Kaveh, M., Amiri Chayjan, R., Taghinezhad, E., Rasooli Sharabiani, V., & Motevali, A. (2020). Evaluation of specific energy consumption and GHG emissions for different drying methods (case study: *Pistacia atlantica*). *Journal of Cleaner Production*, 259, 120963. <https://doi.org/10.1016/j.jclepro.2020.120963>
- Kaveh, M., Jahanbakhshi, A., Abbaspour-Gilandeh, Y., Taghinezhad, E., & Moghimi, M. B. F. (2018). The effect of ultrasound pre-treatment on quality, drying, and thermodynamic attributes of almond kernel under convective dryer using ANNs and ANFIS network. *Journal of Food Process Engineering*, 41(7), e12868. <https://doi.org/10.1111/jfpe.12868>
- Khoshnevisan, B., Rafiee, S., Omid, M., & Mousazadeh, H. (2013). Reduction of CO<sub>2</sub> emission by improving energy use efficiency of greenhouse cucumber production using DEA approach. *Energy*, 55, 676–682. <https://doi.org/10.1016/j.energy.2013.04.021>
- Kian-Pour, N., & Karatas, S. (2019). Impact of different geometric shapes on drying kinetics and textural characteristics of apples at temperatures above 100 °C. *Heat and Mass Transfer*, 55, 3721–3732. <https://doi.org/10.1007/s00231-019-02691-1>
- Koukouch, A., Idlimam, A., Asbik, M., Sarh, B., Izrar, B., Bostyn, S., ... Amine, A. (2017). Experimental determination of the effective moisture diffusivity and activation energy during convective solar drying of olive pomace waste. *Renewable Energy*, 101, 565–574. <https://doi.org/10.1016/j.renene.2016.09.006>
- Mohammad, Kaveh, & Yousef, Abbaspour-Gilandeh Impacts of hybrid (convective-infrared-rotary drum) drying on the quality attributes of green pea. *J of food process engineering*, <https://onlinelibrary.wiley.com/doi/full/10.1111/jfpe.13424>
- Mohammadi, I., Tabatabaekoloo, R., & Motevali, A. (2019). Effect of air recirculation and heat pump on mass transfer and energy parameters in drying of kiwifruit slices. *Energy*, 170, 149–158. <https://doi.org/10.1016/j.energy.2018.12.099>
- Motevali, A., Jafari, H., & Hashemi, S. J. (2018). Effect of IR intensity and AIR temperature on exergy and energy at hybrid infrared- hot AIR dryer. *Chemical Industry & Chemical Engineering Quarterly*, 24(1), 31–42. <https://doi.org/10.2298/CICEQ170123015M>
- Motevali, A., & Minaee, S. (2012). Effects of microwave pretreatment on the energy and exergy utilization in thin-layer drying of sour pomegranate arils. *Chemical Industry & Chemical Engineering Quarterly*, 18(1), 63–72. <https://doi.org/10.2298/CICEQ110702047M>

- Motevali, A., & Tabatabaei, S. (2017). A comparison between pollutants and greenhouse gas emissions from operation of different dryers based on energy consumption of power plants. *Journal of Cleaner Production*, 154, 445–461. <https://doi.org/10.1016/j.jclepro.2017.03.219>
- Nazari, S., Shahhoseini, O., Sohrabi-Kashani, A., Davari, S., Paydar, R., & Delavar-Moghadam, Z. (2010). Experimental determination and analysis of CO<sub>2</sub>, SO<sub>2</sub> and NO<sub>x</sub> emission factors in Iran's thermal power plants. *Energy*, 35, 2992–2998. <https://doi.org/10.1016/j.energy.2010.03.035>
- Nazghelichi, T., Kianmehr, M., & Aghbashlo, M. (2010). Thermodynamic analysis of fluidized bed drying of carrot cubes. *Energy*, 35, 4679–4684. <https://doi.org/10.1016/j.energy.2010.09.036>
- Nikbakht, A., Motevali, A., & Minaei, S. (2014). Energy and exergy investigation of microwave assisted thin-layer drying of pomegranate arils using artificial neural networks and response surface methodology. *Journal of the Saudi Society of Agricultural Sciences*, 13, 81–91. <https://doi.org/10.1016/j.jssas.2013.01.005>
- Onwude, D. I., Hashim, N., Abdan, K., Janius, R., & Chen, G. (2018). Investigating the influence of novel drying methods on sweet potato (*Ipomoea batatas* L.): Kinetics, energy consumption, color, and microstructure. *Journal of Food Process Engineering*, 41(4), e12686. <https://doi.org/10.1111/jfpe.12686>
- Ouaabou, R., Nabil, B., Hidar, N., Lahnine, L., Idlimam, A., Lamharrar, A., ... Mahrouz, M. (2018). Valorization of solar drying process in the production of dried Moroccan sweet cherries. *Solar Energy*, 172, 158–164. <https://doi.org/10.1016/j.solener.2018.05.079>
- Quispe-Fuentes, I., Vega-Galvez, A., Vasquez, V., Uribe, E., & Astudillo, S. (2017). Mathematical modeling and quality properties of a dehydrated native Chilean berry. *Journal of Food Process Engineering*, 40(3), e12499. <https://doi.org/10.1111/jfpe.12499>
- Rabha, D. K., Muthukumar, P., & Somayaji, C. (2017). Energy and exergy analyses of the solar drying processes of ghost chilli pepper and ginger. *Renewable Energy*, 105, 764–773. <https://doi.org/10.1016/j.renene.2017.01.007>
- Ranjbaran, M., & Zare, D. (2013). Simulation of energetic- and exergetic performance of microwave-assisted fluidized bed drying of soybeans. *Energy*, 59, 484–493. <https://doi.org/10.1016/j.energy.2013.06.057>
- Samani, B., Choobin, S., Ghasemi-Varnamkhashti, M., & Abedi, A. (2018). Analysis of energy consumption and end-use application of rapeseed in an agricultural production system in Izeh-Khuzestan. *Engineering in Agriculture, Environment and Food*, 11(3), 101–108. <https://doi.org/10.1016/j.eaef.2018.02.001>
- Sarker, M. S. H., Ibrahim, M., Abdul Aziz, N., & Punan, M. (2015). Energy and exergy analysis of industrial fluidized bed drying of paddy. *Energy*, 84, 131–138. <https://doi.org/10.1016/j.energy.2015.02.064>
- Sehrawat, R., Nema, P. K., & Kaur, B. P. (2018). Quality evaluation and drying characteristics of mango cubes dried using low pressure superheated steam, vacuum and hot air drying methods. *LWT - Food Science and Technology*, 92, 548–555. <https://doi.org/10.1016/j.lwt.2018.03.012>
- Sun, Y., Zhang, M., & Mujumdar, A. (2019). Berry Drying: Mechanism, pre-treatment, drying technology, nutrient preservation, and mathematical models. *Food Engineering Reviews*, 11, 61–77. <https://doi.org/10.1007/s12393-019-9188-3>
- Surendhar, A., Ivasubramanian, V., Vidhyeswari, D., & Deepanraj, B. (2018). Energy and exergy analysis, drying kinetics, modeling and quality parameters of microwave-dried turmeric slices. *Journal of Thermal Analysis and Calorimetry*, 136, 185–197. <https://doi.org/10.1007/s10973-018-7791-9>
- Taghinezhad, E., Kaveh, M., Jahanbakhshi, A., & Golpour, I. (2020). Use of artificial intelligence for the estimation of effective moisture diffusivity, specific energy consumption, color and shrinkage in quince drying. *Journal of Food Process Engineering*, 43(4), e13358. <https://doi.org/10.1111/jfpe.13358>
- Taheri-Garavand, A., Karimi, F., Karimi, M., Lotfi, V., & Khoobakht, G. (2018). Hybrid response surface methodology-artificial neural network optimization of drying process of banana slices in a forced convective dryer. *Food Science and Technology International*, 24(4), 277–291. <https://doi.org/10.1177/1082013217747712>
- Tham, T. C., Ng, M. X., Gan, S. H., Ghua, L. S., Aziz, R., Chuah, L. A., ... Law, C. L. (2017). Effect of ambient conditions on drying of herbs in solar greenhouse dryer with integrated heat pump. *Drying Technology*, 35(14), 1721–1732. <https://doi.org/10.1080/07373937.2016.1271984>
- Tripathy, P. P. (2015). Investigation into solar drying of potato: Effect of sample geometry on drying kinetics and CO<sub>2</sub> emissions mitigation. *Journal of Food Science and Technology*, 52(3), 1383–1393. <https://doi.org/10.1007/s13197-013-1170-0>
- Wang, W., Li, M., Hassanien, R. H. E., Wang, Y., & Yang, L. (2018). Thermal performance of indirect forced convection solar dryer and kinetics analysis of mango. *Applied Thermal Engineering*, 134, 310–321. <https://doi.org/10.1016/j.applthermaleng.2018.01.115>
- Yogendrasidhar, D., & Setty, Y. P. (2018). Drying kinetics, exergy and energy analyses of Kodo millet grains and fenugreek seeds using wall heated fluidized bed dryer. *Energy*, 151, 799–811. <https://doi.org/10.1016/j.energy.2018.03.089>
- Zhao, F., Han, F., Zhang, S., Tian, H., Yang, Y., & Sun, K. (2018). Vacuum drying kinetics and energy consumption analysis of LiFePO<sub>4</sub> battery powder. *Energy*, 162, 669–681. <https://doi.org/10.1016/j.energy.2018.08.023>
- Ziafroughi, A., & Esfahani, J. A. (2016). A salient reduction of energy consumption and drying time in a novel PV-solar collector-assisted intermittent infrared dryer. *Solar Energy*, 136, 428–436. <https://doi.org/10.1016/j.solener.2016.07.025>

**How to cite this article:** Kaveh M, Karami H, Jahanbakhshi A. Investigation of mass transfer, thermodynamics, and greenhouse gases properties in pennyroyal drying. *J Food Process Eng*. 2020;e13446. <https://doi.org/10.1111/jfpe.13446>